https://doi.org/10.5194/acp-2019-1032
Preprint. Discussion started: 24 January 2020

Atmospheric Chemistry and Physics Discussions

Triplet State Formation of Chromophoric Dissolved Organic Matter in Atmospheric Aerosols: Characteristics and Implications

Qingcai Chen,[a*#] Zhen Mu,[a#] Li Xu,[b] Mamin Wang,[a] Jin Wang,[c] Ming Shan,[d] Xudong Yang,[d] Xingjun Fan,[e] Jianzhong Song,[f] Yuqin Wang,[a] Pengchuan Lin,[g] Lixin Zhang,[a] Zhenxing Shen,[h] Lin Du[b*]

[a] *School of Environmental Science and Engineering, Shaanxi University of Science and Technology, Xi'an 710021, China*

[b] *Environment Research Institute, Shandong University, Qingdao, 266237, China*

[c] *School of Civil Engineering, Beijing Jiaotong University, Beijing 100044, China*

[d] *Department of Building Science, School of Architecture, Tsinghua University, Beijing, 100084, China*

[e] *College of Resource and Environment, Anhui Science and Technology University, 233100 Anhui, China*

[f] *State Key Laboratory of Organic Geochemistry, Guangzhou Institute of Geochemistry, Chinese Academy of Sciences, Guangzhou 510640, China*

[g] *College of Resources and Environment, University of Chinese Academy of Sciences, 100190, Beijing, China*

[h] *Department of Environmental Science and Engineering, Xi'an Jiaotong University, Xi'an 710049, China*

*Corresponding authors:

*(Q. C.) Phone: (+86) 0029-86132765; e-mail: chenqingcai@sust.edu.cn; School of Environmental Science and Engineering, Shaanxi University of Science and Technology, Weiyang District, Xi'an, Shaanxi, 710021, China;

*(L. D.) Phone: (+86) 0532-58631980; e-mail: lindu@sdu.edu.cn; Environment Research Institute, Shandong University, Qingdao, 266237, China

https://doi.org/10.5194/acp-2019-1032
Preprint. Discussion started: 24 January 2020

Atmospheric Chemistry and Physics Discussions

ABSTRACT: There is chromophore dissolved organic matter (CDOM) in the atmosphere, which may form triplet-state chromophoric dissolved organic matter (^{3}CDOM*) to further driving the formation of reactive oxygen species (ROS) under solar illumination. ^{3}CDOM* contributes significantly to aerosol photochemistry and plays an important role in aerosol aging. We quantify the ability to form ^{3}CDOM* and drive the formation of ROS by primary, secondary and ambient aerosols. Biomass combustion has the strongest ^{3}CDOM* generation capacity and the weakest vehicle emission capacity. Ambient aerosol has a stronger ability to generate ^{3}CDOM* in winter than in summer. Most of the triplet states generation conform to first-order reaction, but some of them do not due to the different quenching mechanism. The structural-activity relationship between the CDOM type and the ^{3}CDOM* formation capacity shows that the two types of CDOM identified, which similar to the nitrogen-containing chromophores contributed 88% to the formation of ^{3}CDOM*. The estimated formation rate of ^{3}CDOM* can reach ~100 μmol m^{-3} h^{-1} in the atmosphere in Xi'an, China, which is approximately one hundred thousand-times the hydroxyl radical (•OH) production. This study verified that ^{3}CDOM* drives at least 30% of the singlet oxygen ($^1O_2$) and 31% of the •OH formed by aerosols using the spin trapping and electron paramagnetic resonance technique.

Keywords: Atmospheric Chromophores; Triplet States; Structure-activity Relationship; Excitation-emission matrices spectra (EEMs); Aerosol Photochemistry

TOC Art:

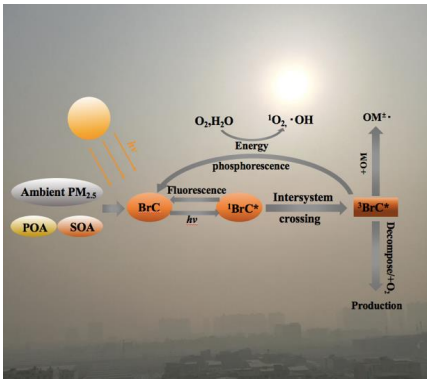

https://doi.org/10.5194/acp-2019-1032
Preprint. Discussion started: 24 January 2020

Atmospheric Chemistry and Physics Discussions

1 Introduction

Aerosols contain organic substances that can absorb sunlight and promote photochemical reactions and have a potentially significant impact on the global climate and atmospheric environmental quality (Borduas-Dedekind et al., 2019; Chen et al., 2016b; Chen et al., 2018; Feng et al., 2013; Rosario-Ortiz & Canonica, 2016). For example, chromophoric dissolved organic matter (CDOM) can be excited under solar illumination to form triplet state chromophoric dissolved organic matter (^{3}CDOM*) through electron transitions and intersystem crossing processes, which can drive the generation of a series of reactive oxygen species (ROS), such as hydroxyl radicals (•OH), superoxide ions (O_2^-) and singlet-state oxygen ($^1O_2$) (Kaur et al., 2019). Thus ^{3}CDOM* has potential effects on multi-phase chemical reactions in atmospheric aerosols (Bodhipaksha et al., 2015; Grebel et al., 2011; Lin et al., 2015).

Previous studies on ^{3}CDOM* are mainly about the water environment, such as sewers, terrestrial natural waters and oceans (Bodhipaksha et al., 2015; Erickson et al., 2018; Zhou et al., 2019), few studies have explored the atmospheric environment. In recent years, the CDOM in atmospheric aerosols, atmospheric fog water and rainfall has been widely found to have a strong photochemical reactivity. (Graedel & Weschler, 1981; Jacob, 1986; Kaur & Anastasio, 2018; Munger et al., 1983). For example, Corral Arroyo et al. (2018) proved that the triplet state has an effect on photochemical reaction and aerosol aging on the particle phase. Kaur et al. (2018) confirmed that CDOM in atmospheric fog water can be excited under solar illumination to form ^{3}CDOM*. Smith et al. (2015) demonstrated that ^{3}CDOM* contributes to secondary organic aerosol (SOA) formation under laboratory simulation conditions. ^{3}CDOM* has a certain chemical reactivity, which leads to its participation in various photochemical reactions (Bluvshtein et al., 2017; Bond et al., 2013; Kloster et al., 2010; Pechony & Shindell, 2010; Sharpless et al., 2014; Zepp et al., 1985). For example, ^{3}CDOM* plays an important role in the oxidation of aniline- and sulfur-containing heterocyclic pollutants (You et al., 2012). ^{3}CDOM* also has the ability to convert O_2 molecules into ROS because the activation energy of ^{3}CDOM* is higher than that of $^1O_2$ (94 kJ mol^{-1}) (Erickson et al., 2018; Rosario-Ortiz & Canonica, 2016). Therefore, it is important to study the formation characteristics and mechanism of ^{3}CDOM* in aerosols to quantify the effect of CDOM on aerosol photochemistry.

https://doi.org/10.5194/acp-2019-1032
Preprint. Discussion started: 24 January 2020


Atmospheric Chemistry and Physics Discussions

^{3}CDOM*, as a reactive intermediate (McNeill & Canonicab, 2016; Wenk et al., 2015), is characterized by instability, complex composition and low concentration. Therefore, it is difficult to quantify its formation characteristics (Graber & Rudich, 2005). Studying the ^{3}CDOM* quenching process by phosphorescence has become an early analysis method. However, it is difficult to quantify the formation process and steady-state concentration of ^{3}CDOM* in this way (Chen et al., 2018; Lin et al., 2015; Turro & Engel, 1969). Because the chemical probe method has the characteristics of avoiding interference with the reaction system and accurate quantification (Lin et al., 2015), the method has become a common method to study the characteristics of ^{3}CDOM* formation. At present, the main chemical probes are dimethoxyphenol, methyl jasmonate, sorbic acid (SA) and 2,4,6-trimethylphenol (TMP) (Bodhipaksha et al., 2015; Lin et al., 2015; Richards-Henderson et al., 2015; Rosario-Ortiz & Canonica, 2016; Kaur & Anastasio, 2018; Moor et al., 2019; Schmitt et al., 2019), with TMP being the most commonly used chemical probe. Lin et al. (2014) showed the reaction ability and transformation mechanism of ^{3}CDOM* formed by humic acid using the TMP probe. Zhou et al. (2019) has reported the ^{3}CDOM* energy distribution using TMP and SA probes. Compared with other chemical probes, TMP contains methyl-substituted groups that can be used as electron donors for ^{3}CDOM* reactions; thus, TMP has a higher reactivity (Canonica & Freiburghaus, 2001). Some substances in the environment can inhibit the reaction between the probes and ^{3}CDOM*, but TMP is not easily affected by these substances (Canonica & Laubscher, 2008; Wenk et al., 2015). Therefore, TMP is suitable as a probe to describe the characteristics of ^{3}CDOM*.

As a precursor of ^{3}CDOM*, CDOM has complex types and compositions. The types and abilities of CDOM to form ^{3}CDOM* may be different, which requires us to analyze both the types and compositions of CDOM. Excitation-emission matrices spectra (EEMs) are a direct method for the characterization of CDOM, allowing identification of the chromophore types by applying parallel factor analysis (PARAFAC), such as humic-like substances (HULIS), quinones, phenols and amino acids (Korak et al., 2014; Ma et al., 2010; McKnight et al., 2001; Rosario-Ortiz & Canonica, 2016; Wenk et al., 2015). Therefore, the EEM method is expected to be used in the structure-activity relationship analysis between the CDOM types and ^{3}CDOM* formation.

https://doi.org/10.5194/acp-2019-1032
Preprint. Discussion started: 24 January 2020

Atmospheric Chemistry and Physics Discussions

The purpose of this study is to examine the formation characteristics and mechanism of ^{3}CDOM* in aerosols under solar illumination conditions. The ^{3}CDOM* formation ability, reaction kinetics and reaction mechanism by different sources of aerosols, including primary organic aerosol (POAs), SOAs and ambient particulate matter (PM) in Xi'an, were studied. The structure-activity relationship between CDOM and ^{3}CDOM* was also studied using the EEM-PARAFAC approach. Finally, the environmental implications of ^{3}CDOM* on aerosol photochemistry were also revealed.

2 Materials and methods

2.1 Sample Collection.

A total of 24 ambient $PM_{2.5}$ samples, 31 POA samples and 22 SOA samples were collected.

The ambient PM samples were collected at the Shaanxi University of Science and Technology, Xi'an, Shaanxi (see Table S1 of SI). The PM samples were collected on quartz fiber filters by an intelligent large-flow particle sampler (Xintuo XT-1025, Shanghai, China) with a sampling time of 23 h 30 min and a sampling flow rate of 1000 L/min. According to the seasonal characteristics of Xi'an, 24 samples were collected from June 24-July 5 (summer) and November 30-December 11 (winter). The filters were stored in a refrigerator at -20 ℃ before analysis.

The sources of POA include vehicle exhaust, cooking, biomass burning and coal combustion (see Table S2 of SI). Six vehicle exhaust samples, including medium- and heavy-sized freight vehicles and busses (national third emission standard), were collected on quartz filters by a customized sampler (Ma et al., 2018). Five cooking samples, including frying (fried eggs with tomatoes and fried meat with salt) and barbecuing (roast mutton, potatoes, squid and duck), were collected on Teflon filters by a four-channel sampler (TH-16A, Tianhong Environmental Protection Industry, Wuhan, China) at a flow rate of 16.7 L/min and a sampling time of 20 min. Crop straw (artemisia, corn straw and corn straw bar-shaped compacted material, etc.), wood (wood and grape branches) and coal (lump coal) samples were burned in farm stoves and collected on quartz filters (tprs-001, Taipuruisi, China) by a sampler (DustTrak 8530, TSI Inc., America). The sampling site is located in Hujiazhuang village, Hu County, Xi'an, Shaanxi. The sampling time is 1 h, and the flow rate is 8.7

https://doi.org/10.5194/acp-2019-1032
Preprint. Discussion started: 24 January 2020

Atmospheric Chemistry and Physics Discussions

L/min. Six straw burning samples, 4 wood burning samples and 3 coal combustion samples were collected using this method. Crop straw (wheat straw, corn straw, rice straw, etc.) and wood (pine and Chinese fir), with 1 mL of alcohol as a combustion promoter, were burned in a resuspension tank and collected by a sampler, thereby replacing the filter every 10 min. Three straw burning samples and 3 wood combustion samples were collected with this method. The crop straw and wood were obtained in rural areas of Liuzhou, Guangxi (Wei et al., 2017; Yang et al., 2013). A combustion sample of honeycomb-shaped coal, which is made by mixing crushed coal with 40% clay, is collected. Honeycomb-shaped coal was ignited outside the mixing box and then moved into the coal stove inside the box. After adding two lumps of honeycomb-shaped coal, the mixing box was closed, and the gas pump was opened for sampling. The coal samples were mainly obtained in Pingdingshan, Henan (Wei et al., 2017; Yang et al., 2013). All samples are stored in a refrigerator at -20 ℃ before analysis.

SOAs were obtained by oxidation of different volatile organic compounds (VOCs) under different conditions (see Table S3 of SI) (Liu et al., 2018). The precursor VOCs were limonene (LIM), α-pinene (APIN), toluene (TOL) and naphthalene (NAP). SOAs with low, moderate and high oxidation degrees are obtained by controlling the concentrations of O_3, •OH and NO_X in the reaction and the illumination conditions. The methods of achieving low, moderate and high oxidation degrees are as follows: (1) Low-oxidation conditions (LO): VOCs are loaded into the reaction system by purified dry air. A high concentration of cyclohexane is used as a masking agent for •OH. Under pure oxygen flow conditions, O_3 is produced by a high voltage current, and VOCs are oxidized by O_3. (2) Moderate-oxidation conditions (MO): •OH is produced by photolysis of H_2O_2. NO is added to achieve a high NO_X concentration, and VOCs are oxidized by NO_X. (3) High-oxidation conditions (HO): Excess O_3 is an oxidation condition. The reaction time is not shorter than 6 h to ensure the complete reaction of VOCs. Twenty-two SOA samples were collected by a low-pressure impact sampler (DLPI+, Dekati Ltd., Finland) with a sampling time of 1.5 h.

2.2 Sample Extraction.

Particle matter on filter was ultrasonically extracted for 15 min in a clean brown glass bottle containing ultrapure water (>18.2 MΩ•cm, Master series, Hitech, China), and water-soluble organic matter (WSOM) extractions were obtained through a 0.45-μm

https://doi.org/10.5194/acp-2019-1032
Preprint. Discussion started: 24 January 2020

Atmospheric Chemistry and Physics Discussions

filter (Jinteng, China). Background extractions were also obtained using blank filters with the same method as that used for the sample extracts.

2.3 TOC Analysis.

A volume of 0.5 mL extracted WSOM was diluted to a concentration of 0.1-10 mg/L with ultrapure water. The water-soluble organic carbon (WSOC) from extraction was quantitatively analyzed by a total organic carbon (TOC) analyzer (Sievers M9, General Electric, America) in CO_2 removal mode. To avoid WSOC concentration changes caused by sample exposure to air and time prolongation, all extractions must be quantitatively analyzed within 30 min after extraction. To avoid background interference, background samples are also analyzed before each batch of samples is analyzed. Before and after sample analysis, standard curves of a series of glucose standard solutions (0, 0.05, 0.1, 0.2, 0.5, 1, 5 and 10 mg/L) were also measured. Based on the off-line analysis mode of the TOC analyzer, each sample was continuously analyzed 3 times, and the average value after subtracting the background value was the final detection value. The relative standard deviation of the WSOC content was 1.5%.

2.4 Optical Absorption and EEM Fluorescence Spectra.

Absorption and EEMs of the extracts were obtained using a fluorescence spectrophotometer (Aqualog, Horiba Science, America). Detection conditions: the excitation wavelength range is 200-600 nm and the emission wavelength range is 250-800 nm. The wavelength interval is 5 nm, and the integration time is 0.5 s. The background samples are also analyzed under the same detection conditions and deducted from the sample signal. The WSOC concentration in the sample was diluted to within 10 ppm so that the absorbance at 250 nm was less than 0.5. The inner filter effect has little influence on the results because the sample was fully diluted. Correction of the inner filter effect for the EEMs is also performed.

2.5 Triplet State Formation Experiments.

Triplet state formation experiments are carried out in a customized reactor (Figure S1 of the SI). The material of the reactor is high-purity quartz. A high-purity quartz plate is arranged at the top of the reactor. The upper edge of the reactor is embedded with a rubber gasket, which allows sealing through clamping with the quartz plate. The upper part of the reactor has two air vents for injecting clean air. Two holes at the bottom of the reactor are connected with a water-cooled circulator to ensure that the

https://doi.org/10.5194/acp-2019-1032
Preprint. Discussion started: 24 January 2020


Atmospheric Chemistry and Physics Discussions

ambient temperature and humidity in the reactor are approximately 25 ℃ and 50%, respectively. The reactor is placed on a magnetic agitator, and a rotation rate of 200 rpm is used to assist in stabilizing the temperature and humidity in the reactor. The reaction was carried out in a customized quartz tank, in which 4 circular cells with a radius of 5.6 mm and depth of 2.5 mm were set on a square quartz plate with an area of 35×35 mm^2. The customized quartz tank is placed in the reactor, and the bottom and upper edges are in contact with the water surface and air, respectively. The illumination device is a xenon lamp with a VISREF filter (PLS-SXE 300, Perfectlight, China; Figure S2 of the SI shows the wavelength spectrum of illumination). The illumination intensity per unit area of the xenon lamp is approximately 1.2-1.3 times that of sunlight at 12:00 (N34°22′35.07″, E108°58′34.58″).

Volumes of 135 μL WSOM extract (Tables S1-S3 of the SI show the WSOC concentration information) and 25 μL TMP solution (c_{TMP} = 4 mM) are mixed in the reaction cell and reacted under simulated solar illumination. The illumination times are 0, 5, 10, 15, 30, 45, 60 and 90 min. Samples were collected at different times. Then, 20 μL phenol solution (c_{phenol} = 4 mM), as an internal standard for quantifying the TMP peak area of liquid chromatography, was added to the collected sample. Compared with the previous study, the concentration of TMP used in the paper is higher; therefore, we compared high-concentration TMP with low-concentration TMP. The results show that under our reaction conditions, the high-concentration TMP may have a relatively low background and a higher reaction rate constant (the results are shown in Figure S3 of SI).

The sulfate in aerosols may produce sulfate free radicals under illumination, which can possibly consume TMP. Simulated TMP consumption by a sulfate ion solution was also examined in this study. Three parallel groups of background and control experiments are compared. We studied the effect of salts on the formation of triplet states. As shown in Figure S4, in the reaction system with or without $(NH_4)_2SO_4$, no significant difference exists in the decay rate of TMP. To further study the effect of salts on the formation system of triplet states, we used solid-phase extraction to separate high-polar substance salts and low-polar HULISs (Chen, et al., 2016a). We determined the effects of salts, HULISs, and a salt and HULIS mixture on TMP attenuation. As shown in Figure S5, we found that when the salts were mixed with

https://doi.org/10.5194/acp-2019-1032
Preprint. Discussion started: 24 January 2020

Atmospheric Chemistry and Physics Discussions

low-polar substances, no significant effect on TMP attenuation was identified in the low-polar reaction system.

Ultra-high-performance liquid chromatography (UPLC, Acquity UPLC H-Class, Waters, America) was conducted to quantify the TMP concentration of the above samples. The UPLC analysis conditions were as follows. The mobile phase consisted of 50% acetonitrile and 50% water and had a flow rate of 0.1 mL/min; the ultraviolet detector used a detection wavelength of 210 nm. Each batch of samples contained internal and external standard solutions, background samples, control samples and WSOC extraction samples. The relative standard deviation of the TMP content is 8.8%.

2.6 ROS Capture Experiments.

(1) The driving effects of the triplet state on $^1O_2$ were studied. 2,2,6,6-tetramethyl-piperidine (TEMP, c_{TEMP} = 0.25 M) was used as a scavenger for $^1O_2$, and SA (c_{SA} = 4×10^2 μM) was added into the reaction system as a triplet state quencher. After 60 min of illumination (the illumination device is shown in Figure S1 of the SI), the $^1O_2$ signal was detected by an electron paramagnetic resonance (EPR) spectrometer (MS5000, Freiberg) and compared with the content of $^1O_2$ under the condition of the presence or absence of a quencher of the triplet state. (2) The driving effects of the triplet state on •OH were studied. 5,5-dimethyl-1-pyrroline-N-oxide (DMPO, c_{DMPO} = 0.1 M) was used as a scavenger for •OH. L-Histidine ($c_{L\text{-}Histidine}$ = 0.1 M) was used as a quencher for $^1O_2$. After 60 minutes of illumination, the content of •OH was compared under the condition of the absence or presence of a quencher of the triplet state. The content of •OH was also compared in the condition of the absence or presence of a quencher of $^1O_2$.

2.7 Data Analysis.

Kaur and Anastasio (2018) and Richards-Henderson et al. (2015) reported that the consumption characteristics of the probe conformed to first-order kinetics in the reaction to form the triplet state. In this study, the value of k_{TMP} is the attenuation rate constant of TMP, which is used to calculate the yield of the triplet state in ambient atmosphere. The first-order kinetics equation is used to fit the exponential relationship among k_{TMP}, the concentration of TMP (c_{TMP}) and the illumination time (t):

$$c_{TMP} = ae^{tk_{TMP}} \quad (1)$$

https://doi.org/10.5194/acp-2019-1032
Preprint. Discussion started: 24 January 2020

Atmospheric Chemistry and Physics Discussions

To evaluate the contribution of different chromophore types to triplet formation and to study the structure-activity relationship between the chromophores and triplet formation, the PARAFAC method was used to analyze the consumption rate constants of TMP coupled with EEM data sets. The developed model not only identifies the types of CDOM but also identifies the relative contributions of the different types of CDOM to the formation of ^{3}CDOM*. The basic principles and equations of the model are as follows:

$$X_{n,i,j} = \sum_{f=1}^{F} a_{n,f} \cdot \left(b_{i,f} c_{j,f}\right) + e_{n,i,j} \quad (2)$$

where n is the number of samples for n = 1,... N; i = 1... I; j = 1,... J; k = 1,... K; $X_{n,i,j}$ are the EEM ($X_{n,\ 1\ldots\ I\text{-}1,1\ldots\ J\text{-}1}$) coupled data sets of the consumption rate constants of the TMP (k_{TMP}) values $X_{n,I,J}$; f is the number of factors; a is the factor load coefficient; b and c contain factor spectrum information; and $e_{n,i,j}$ are the model residuals.

The EEM data sets coupled with k_{TMP} values are analyzed through the drEEM toolbox (http://www.models.life.ku.dk/dreem). Detailed model analysis has been reported in previous studies by Chen et al. (2016b; 2016c). According to the EEM characteristics of the 2- to 10-component PARAAFAC models and the trend of the residual error, a 5-component PARAFAC model were selected.

3 Results and discussion

3.1 Reaction Kinetics of ^{3}CDOM* Formation.

The kinetics characteristics of ^{3}CDOM* formed by different source aerosols are studied. Figure 1 (A) and (C) illustrate the variation of the TMP concentration under simulated solar illumination, where (i), (ii) and (iii) are the average TMP consumption of the POA, SOA and ambient PM samples, respectively. The results show that the consumption of TMP in most samples conforms to the first-order kinetics equation (Kaur & Anastasio, 2018), which indicates that the concentration of the triplet state formed in the reaction system is constant and the formation rate of ^{3}CDOM* is the same as its quenching rate. In this case, the quenching mechanism of ^{3}CDOM* conforms to the paths (2)-(3) and (5)-(7) described in Scheme 1. In the reaction process, ^{3}CDOM* may not be consumed, but ^{3}CDOM* mainly promotes energy transfer, such as converting O_2 to $^1O_2$.

As shown in Figure 1C, in contrast to the above results, the consumption of TMP of certain vehicle exhaust and biomass combustion samples do not completely conform

https://doi.org/10.5194/acp-2019-1032
Preprint. Discussion started: 24 January 2020

Atmospheric Chemistry and Physics Discussions

to first-order reaction kinetics. Specifically, the consumption of TMP within 0-20 min of the reaction stage conforms to first-order reaction kinetics. With the reaction proceeding, the consumption of TMP changes to zero-order reaction kinetics after 20 min. The difference in TMP consumption kinetics reflects the difference in the quenching mechanisms of ^{3}CDOM*. The results show that the reaction rate is mainly controlled by the TMP concentration and that the ^{3}CDOM* concentration remains constant because more ^{3}CDOM* is formed in the initial stage. With the reaction proceeding, CDOM in the sample undergoes an irreversible photochemical reaction, which results in the loss of CDOM in the reaction system so that the steady-state concentration of ^{3}CDOM* decreases. In this case, the mechanisms conform to the paths (1) and (4) described in Scheme 1. Whether CDOM changes the molecular properties during the process of ^{3}CDOM* formation depends on its molecular structure, as well as the type of CDOM, which is discussed in section 3.3.

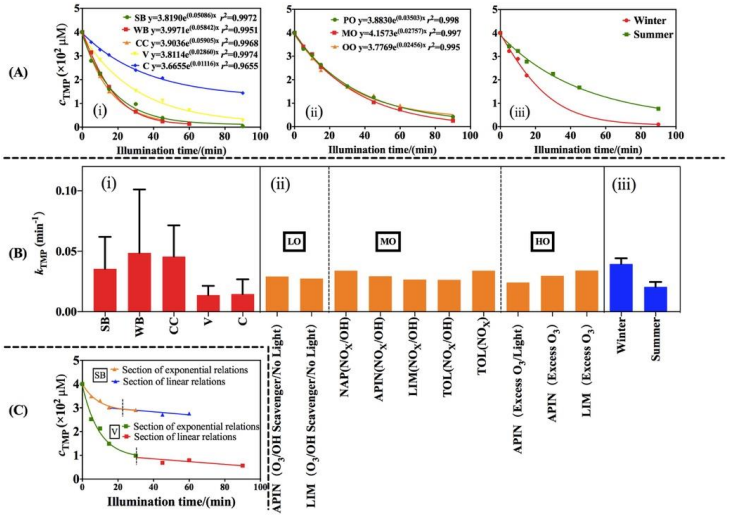

Figure 1. Reaction kinetics and formation rate of ^{3}CDOM* of different source aerosols. (A) The average consumption of TMP of aerosols from different sources conforms to first-order reaction kinetics. (B) Comparison of the average rates of ^{3}CDOM formation of aerosols from different sources. (C) The average consumption of TMP by aerosols does not conform to first-order kinetics. (i) POAs. (ii) SOAs. (iii) Ambient PM. SB is straw burning, CC is coal combustion, WB is wood burning, V is vehicle exhaust and C is cooking. LO, MO and HO indicate low oxidation, moderate oxidation and high oxidation, respectively.

https://doi.org/10.5194/acp-2019-1032
Preprint. Discussion started: 24 January 2020

Atmospheric Chemistry and Physics Discussions

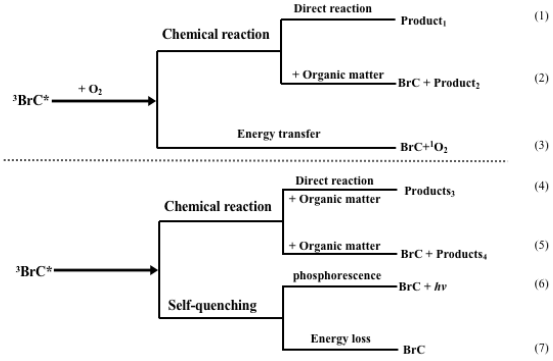

Scheme 1. The Quenching Mechanism of ^{3}CDOM*.[1]

3.2 Comparison of the ^{3}CDOM* Formation Ability of Aerosols Different Sources.

The ^{3}CDOM* formation ability of different sources aerosols is different. As shown in Figure 1B, There is no significant difference of k_{TMP} in POA, SOA and ambient PM on average, the values of k_{TMP} were 0.032±0.032, 0.030±0.005 and 0.030±0.011 min^{-1}, respectively. However, significant differences in the k_{TMP} values of POAs were found, which may be related to the large number of aromatic organic compounds produced by combustion, such as resorcinol, indole and other typical CDOM, which have a high photochemical activity (Wong et al., 2017; Glasius et al., 2006; Mcdonald et al., 2000). Straw and wood burning both belong to biomass combustion, the k_{TMP} values of the straw burning samples are lower than those of the wood burning samples (0.035 min^{-1}). Straw burning results in large quantities of phenolic substances (Rogge et al., 1998; Schauer et al., 2001), while phenol-like chromophores do not contribute significantly to TMP consumption, as discussed in detail in section 3.3. The k_{TMP} values of vehicle exhaust were the lowest (0.013 min^{-1}), which were similar to cooking samples. N-alkanes, carboxylic acids and alkanols, which do not produce ^{3}CDOM*, are the most important markers of vehicle exhaust (Ho et al., 2009; Lee et al., 2001; Tian et al., 2009). In addition, aliphatic aldehydes and ketones account for the highest proportion of the cooking emissions in China, reaching more than 70% (Xu et al., 2017). These aliphatic compounds cannot form ^{3}CDOM*, which lead to the low k_{TMP} values of the vehicle exhaust and cooking samples.

https://doi.org/10.5194/acp-2019-1032
Preprint. Discussion started: 24 January 2020

Atmospheric Chemistry and Physics Discussions

The k_{TMP} values of SOAs formed under different oxidation conditions are similar, and the average value is 0.029 min^{-1}. The results indicate that the photochemical reactivity of SOAs does not depend mainly on the precursors and oxidation degree. The SOA samples formed by TOL under NO_X oxidation conditions have a slightly higher k_{TMP} value (~1.3 times) than those formed under NO_X/•OH conditions, which indicates that the CDOM formed by NO_X may have a relatively higher photochemical reactivity, but the effect is limited.

The k_{TMP} value of the ambient PM in winter (0.040±0.005 min^{-1}) is approximately 2-times higher than that in summer (0.021±0.004 min^{-1}) in Xi'an, which indicate that considerable differences exist in the types and contents of CDOM in winter and summer. Shen et al. (2017) reported that the strong light absorption substances in organic aerosols are a mixture of biomass burning and coal combustion emissions in Xi'an. Increased coal combustion results in a higher content of CDOM in winter, and CDOM from coal combustion has higher k_{TMP} values, as shown in Figure 1B. On the other hand, the most sensitive CDOM bleached or decomposed due to the high solar illumination intensity in summer (Wong et al., 2019; Helms et al., 2008; Sharpless et al., 2014), which results in the reduction of CDOM with photochemical reactivity. Therefore, the ability of the ambient PM to form ^{3}CDOM* is greater in winter. In particular, the highest k_{TMP} value was 0.046 min^{-1} in the winter samples, which was similar to coal combustion and wood burning samples. This result is consistent with the fact that coal combustion is an important source of ambient PM in winter in Xi'an.

3.3 Structure-activity Relationship Between the CDOM Types and ^{3}CDOM* Formation.

The characteristics of ^{3}CDOM* formation depend on the chemical structure of CDOM. Absorption spectra can provide some structural characteristics of CDOM (Figure S6). For example, E_2/E_3 (Abs_{250nm}/Abs_{365nm}) values represent the aromaticity and molecular weight of organic aerosols (Peuravuori & Pihlaja, 1997). Figure 2 shows the E_2/E_3 characteristics in the different samples. The E_2/E_3 values of the POA, SOA and ambient PM samples were 6.51±3.55, 17.57±9.24 and 5.29±0.39, respectively. As shown in Figure 3 (i)-(iii), the results show that k_{TMP} has a negative correlation with E_2/E_3 and a positive correlation with the mass absorption efficiency (MAE) in all sample types. In general, a smaller E_2/E_3 value and a high MAE value indicate greater aromaticity and a higher molecular weight (Duarte et al., 2005). The

https://doi.org/10.5194/acp-2019-1032
Preprint. Discussion started: 24 January 2020

Atmospheric Chemistry and Physics Discussions

results indicate that greater CDOM aromaticity corresponds to a greater ^{3}CDOM* formation ability.

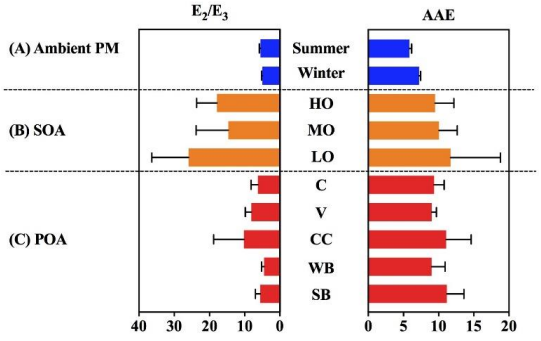

Figure 2. The characteristics of the AAE and E_2/E_3 ratio of different types of aerosols.

The absorption Angström-exponent (AAE) is also a useful parameter for representing the chemical structure of CDOM (Wu et al., 2019). A larger AAE value indicates a higher polarity of CDOM and degree of oxidation (Chen et al., 2016b). The AAE values range from 5.8 to 11.7 for all samples in the wavelength range of 365-550 nm in this study (Figure 2). Additionally, the AAE values of the POA and SOA samples were found to have a weak negative correlation with k_{TMP} (r=0.29, p<0.1235; r=0.19, p<0.4207), while the AAE values of the ambient PM samples had a significant positive correlation with k_{TMP} (r=0.86, p<0.0001, Figure 3 (d)-(f)). The results indicate that CDOM with a higher polarity or oxidation degree in ambient PM has a higher ^{3}CDOM* formation ability, but the CDOM in POA and SOA samples with a higher polarity or oxidation degree may have a lower ^{3}CDOM* formation ability.

https://doi.org/10.5194/acp-2019-1032
Preprint. Discussion started: 24 January 2020

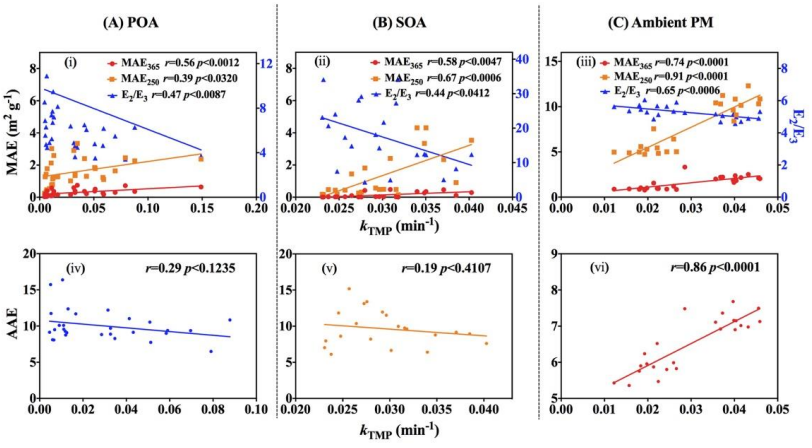

Figure 3. The characteristics of the correlation between k_{TMP}, the AAE, and the E_2/E_3 ratio. (i), (ii) and (iii) show the correlations between k_{TMP}, MAE and E_2/E_3. (iv), (v) and (vi) show the correlations between k_{TMP} and the AAE. (A), (B) and (C) are POA, SOA and ambient PM sample results, respectively.

The ^{3}CDOM* formation ability depends on the CDOM type. In this study, five types of CDOM were identified through the PARAFAC model, as shown in Figure 4C and E, and Figure 4A shows the relative contents of CDOMs in the different samples. The C1 and C3 CDOM peaks appear at Ex./Em. = 220/350 and 275/350 nm and at Ex./Em. = 230/306 and 280/306 nm, respectively, which are similar to those of tryptophan and the CDOM driven by the Maillard reaction. These peaks may be attributed to N-containing compounds (Gao & Zhang, 2018). The average content of C1 and C3 in all samples is small at only 8%. In contrast, C2 and C4 are the two CDOMs that contribute the most to fluorescence, reaching 36% and 50%, respectively, and their emission wavelengths are 352 and 430 nm, respectively, which are similar to those of less and highly oxygenated HULISs (Chen et al., 2016c; Coble, 2007; Fellman et al., 2009; Murphy et al., 2008; Wu et al., 2019). C5 contributes to the fluorescence of all samples, but only 5% on average. C5 peaks appear at Ex./Em.= 220/295 and 275/295 nm, which may be attributed to phenol-like species.

https://doi.org/10.5194/acp-2019-1032
Preprint. Discussion started: 24 January 2020

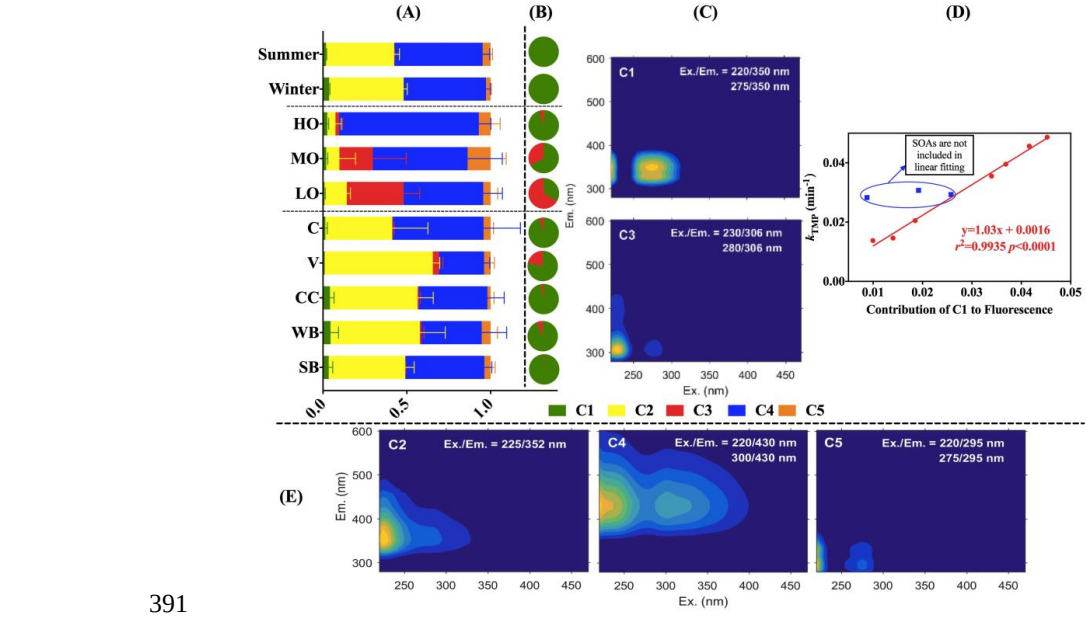

Figure 4. Types of CDOM and their contributions to ^{3}CDOM*. (A) Different CDOM types contributing to fluorescence. (B) Difference in CDOM contributions to ^{3}CDOM*. (C) EEM profiles of C1 and C3. (D) Linear relationship between the contribution of C1 to fluorescence and k_{TMP}. (E) EEM profiles of C2, C4 and C5.

The ability of different CDOM to form ^{3}CDOM* is different. The structure-activity relationship between the CDOM type and ^{3}CDOM* formation rate was established by the improved PARAFAC model in equation (2). Figure 4B illustrates the relative contributions of the different types of CDOM to the total formation rate of ^{3}CDOM*. ^{3}CDOM* formed by C1 and C3 contributes significantly, with average contributions of 88% and 12%, respectively. In LO-, MO- and HO-SOAs, the contributions of C1 to fluorescence are 0.9%, 1.9% and 2.5%, respectively, and the contributions to ^{3}CDOM* are 33.6%, 66.8% and 95.2%, respectively. That indicates that ^{3}CDOM* formation of C1 is promoted by the increase in the oxidation degree. With increasing oxidation degree, the content of C3 decreases, which indicates that C3 is oxidized and decomposed (Wong et al., 2015). C2, C4 and C5 do not contribute significantly to ^{3}CDOM* formation in all samples.

The energy levels of different ^{3}CDOM* is different. TMP, as a triplet-state probe used in this study, has remarkable electron transfer characteristics and is related to the energy of ^{3}CDOM* (Zhou et al., 2019). Approximately 70% of high-energy ^{3}CDOM*

https://doi.org/10.5194/acp-2019-1032
Preprint. Discussion started: 24 January 2020

Atmospheric Chemistry and Physics Discussions

was reportedly found in municipal wastewater using TMP as a triplet-state probe (Zhou et al., 2019). Most ^{3}CDOM* has both the ability to capture TMP by electron transfer and to transfer energy to form $^1O_2$ (Bodhipaksha et al., 2015; McNeill & Canonicab, 2016; Zhou et al., 2019). However, high-energy ^{3}CDOM* has a greater ability of transferring electrons (Kaur & Anastasio, 2018; Zhou et al., 2019). According to the contribution of ^{3}CDOM* to TMP consumption, the results of this study indicated that the ^{3}CDOM* formed by HULISs and phenol-like substances are not able to transfer electrons. The quenching mechanism is mainly energy transfer, which means that this ^{3}CDOM* has more significant effect of driving ROS. However, typical N-containing chromophores such as amino acids may include both of the above quenching modes. Figure 3D illustrates that the contribution of C1 to fluorescence in the POA and ambient PM samples is positively correlated with k_{TMP}, indicating that C1 is the most important high-energy ^{3}CDOM* precursor in aerosols.

4 Environmental implication

This study illustrates the ^{3}CDOM* formation characteristics and mechanisms of CDOM in aerosols. We confirm that different aerosols have the ability to form ^{3}CDOM* so that atmospheric CDOM has the potential to contribute to the photochemical aging process of aerosols. For example, Coal combustion and wood burning aerosols has the highest ^{3}CDOM* formation ability. The results indicate that the photochemical reactivity of aerosols from different sources is different, and that an external mixing state of photochemical aging level exists. Based on the results of this study, we roughly calculate the relative contribution of ^{3}CDOM* to aerosol oxidation in Xi'an, China, as shown in Table S1. The ^{3}CDOM* formation rate ranges from 52 to 194 μmol m^{-3} h^{-1} in this study, and the reported lifetime of ^{3}CDOM* is approximately 2-80 μs (Rosario-Ortiz & Canonica, 2016). Compared with ^{3}CDOM*, •OH is recognized as an important oxidant in aerosols. The photochemical formation rate of •OH is approximately (0.32-3.0) × 10^{-3} μmol m^{-3} h^{-1}, and the lifetime of •OH is approximately 5-10 μs (Das, 2009; Faust & Allen, 1993; Lambe et al., 2007). As stated above, the results show that the ^{3}CDOM* formation rate roughly one hundred thousand-times the •OH production, although the ^{3}CDOM* reaction activity may be thousands of times lower than that of •OH. We noted that ^{3}CDOM*-involved reactions have a potentially important contribution to the photochemical process of

https://doi.org/10.5194/acp-2019-1032
Preprint. Discussion started: 24 January 2020

Atmospheric Chemistry and Physics Discussions

atmospheric aerosols, which may be matched by that of •OH. ^{3}CDOM* has been reported to have a stronger oxidation effect on phenols and to have a significant effect on the formation of SOAs (Smith et al., 2015).

In additional experiments, we verify the ability of ^{3}CDOM* to drive ROS formation, including $^{1}O_2$ and •OH (Manfrin et al., 2019). As shown in Figure 5, the result shows that the signal strength of $^{1}O_2$ decreases by 30% when the ^{3}CDOM* is quenched by SA (comparing Figure 5 (c) and (d)). As shown in Figure 6, the result shows that the signal strength of •OH decreases by 31% when the ^{3}CDOM* is quenched by SA (comparin Figure 6 (c) and (d)). We also found that the signal strength of •OH decreases by 71% when $^{1}O_2$ is quenched by L-histidine (comparing Figure 6 (c) and (e)). According to the above results, ^{3}CDOM* drives at least 30% of the $^{1}O_2$ and 31% of the •OH in water-soluble PM. Therefore, we speculate that ^{3}CDOM* may be a potential important driving factor for aerosol aging. This study also shows that the aerosols from different sources have different ^{3}CDOM* formation abilities.

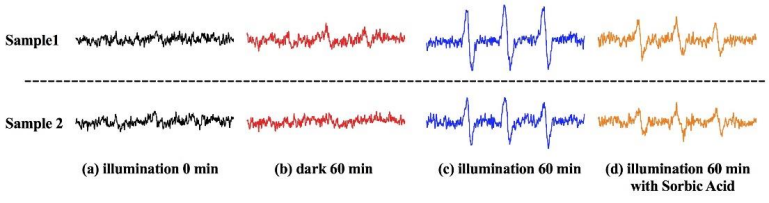

Figure 5. The effect of triplet states driving $^{1}O_2$. Sample 1 and Sample 2 are water extractions of two different particulate matter samples. The particulate matter of Sample 1 and Sample 2 was collected on December 12 and 13, 2017, respectively. The concentrations of WSOC are both 20 mg/L.

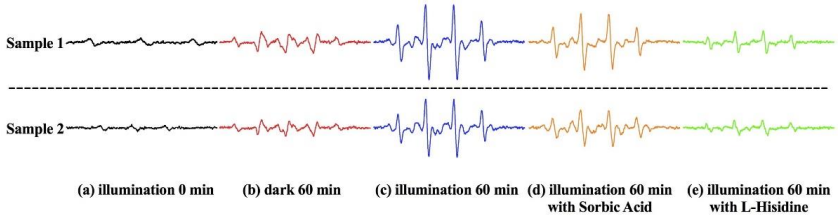

Figure 6. The effect of triplet states driving •OH. Sample 1 and Sample 2 are water extractions of two different particulate matter samples. The particulate matter of Sample 1 and Sample 2 wasa collected on December 12 and 13, 2017, respectively. The concentrations of WSOC are both 20 mg/L.

https://doi.org/10.5194/acp-2019-1032
Preprint. Discussion started: 24 January 2020

In this study, the structure-activity relationship between the CDOM type and ^{3}CDOM* formation rate was established by the EEM-PARAFAC approach. We identify that the C1 and C3 chromophores, which may be attributed to N-containing substances, significantly contribute to ^{3}CDOM* formation, although C1 and C3 contribute little to the total fluorescence intensity. The results showed that C1 and C3 chromophores are the main precursors for the formation of ^{3}CDOM* in aerosols. In contrast, HULIS and phenol-like chromophores do not contribute significantly to TMP attenuation. However, the above do not mean that these substances do not have the ability to form ^{3}CDOM*. In this case, as shown in Scheme 1, ^{3}CDOM* through self-quenching and energy transfer does not consume TMP, and low-energy ^{3}CDOM* cannot react with TMP.

Data availability

The $PM_{2.5}$ data used in this paper are from http://www.cnemc.cn (China National Environmental Monitoring Center).

Supporting information

Additional details, including Tables S1−S3, Figures S1−S10, calculation of the formation rate of ^{3}CDOM* and the consumption rate of TMP due to ^{3}CDOM* formation in aerosols under solar illumination, are contained in the SI.

Author information

Corresponding authors:
*Q.C., phone/fax: 0086-0029-86132765; e-mail: chenqingcai@sust.edu.cn;
*L.D., phone/fax: 0086-0532-58631980; e-mail: lindu@sdu.edu.cn.
Author contributions:
#Q.C. and Z.M. contributed equally to this work.

Acknowledgments

This work was supported by the National Natural Science Foundation of China (grant numbers 41877354, 41703102 and 91644214) and the Shandong Natural Science Fund for Distinguished Young Scholars (JQ201705).

https://doi.org/10.5194/acp-2019-1032
Preprint. Discussion started: 24 January 2020

Atmospheric Chemistry and Physics Discussions

References

Bluvshtein, N., Lin, P., Flores, J. M., Segev, L., Mazar, Y., Tas, E., Snider, G., Weagle, C., Brown, S. S., Laskin, A. and Rudich, Y: Broadband optical properties of biomass-burning aerosol and identification of brown carbon chromophores, J. Geophys. Res.-Atmos., 122, 5441-5456, http://doi.org/10.1002/2016JD026230, 2017.

Bodhipaksha, L. C., Sharpless, C. M., Chin, Y. P., Sander, M., Langston, W. K., and MacKay, A. A.: Triplet Photochemistry of Effluent and Natural Organic Matter in Whole Water and Isolates from Effluent-Receiving Rivers, Environ. Sci. Technol., 49, 3453-3463, http://doi.org/10.1021/es505081w, 2015.

Bond, T. C., Doherty, S. J., Fahey, D. W., Forster, P. M., Berntsen, T., DeAngelo, B. J., Flanner, M. G., Ghan, S., Kaercher, B., Koch, D., Kinne, S., Kondo, Y., Quinn, P. K., Sarofim, M. C., Schultz, M. G., Schulz, M., Venkataraman, C., Zhang, H., Zhang, S., Bellouin, N., Guttikunda, S. K., Hopke, P. K., Jacobson, M. Z., Kaiser, J. W., Klimont, Z., Lohmann, U., Schwarz, J. P., Shindell, D., Storelvmo, T., Warren, S. G., and Zender, C. S.: Bounding the role of black carbon in the climate system: A Scientific assessment, J. Geophys. Res.-Atmos., 118, 5380-5552, http://doi.org/10.1002/jgrd.50171, 2013.

Borduas-Dedekind, N., Ossola, R., David, R. O., Boynton, L. S., Weichlinger, V., Kanji, Z. A. and McNeill, K.: Photomineralization mechanism changes the ability of dissolved organic matter to activate cloud droplets and to nucleate ice crystals, Atmos. Chem. Phys., 19, 12397–12412, https://doi.org/10.5194/acp-19-12397-2019, 2019.

Canonica, S., and Freiburghaus, M.: Electron-Rich Phenols for Probing the Photochemical Reactivity of Freshwaters, Environ. Sci. Technol., 35, 690-695, http://doi.org/10.1021/es0011360, 2001.

Canonica, S., and Laubscher, H. U.: Inhibitory effect of dissolved organic matter on triplet-induced oxidation of aquatic contaminants, Photochem. Photobio. Sci., 7, 547-551, http://doi.org/10.1039/b719982a, 2008.

Chen, Q. C., Ikemori, F., Higo, H., Asakawa, D., and Mochida, M.: Chemical Structural Characteristics of HULIS and Other Fractionated Organic Matter in Urban Aerosols: Results from Mass Spectral and FT-IR Analysis, Environ. Sci. Tech., 50(4), 1721-1730. http://doi.org/10.1021/acs.est.5b05277, 2016a.

Chen, Q. C., Ikemori, F., and Mochida, M.: Light Absorption and Excitation–Emission Fluorescence of Urban Organic Aerosol Components and Their Relationship to Chemical Structure, Environ. Sci. Tech., 50, 10859-10868, http://doi.org/10.1021/acs.est.6b0254, 2016b.

Chen, Q. C., Miyazaki, Y., Kawamura, K., Matsumoto, K., Coburn, Sean., Volkamer, R., Iwamoto, Y, Kagami, S, Deng, Y. G., Ogawa, S., Ramasamy, S., Kato, S., Ida, A., Kajii, Y., and Mochida, M.: Characterization of Chromophoric Water-Soluble Organic Matter in Urban, Forest, and Marine Aerosols by HR-ToF-AMS Analysis and Excitation-Emission Matrix Spectroscopy, Environ. Sci. Tech., 50, 10351-10360, http://doi.org/10.1021/acs.est.6b01643, 2016c

Chen, Y., Zhang, X., and Feng, S. X.: Contribution of the Excited Triplet State of Humic Acid and Superoxide Radical Anion to Generation and Elimination of Phenoxyl Radical, Environ. Sci. Tech., 52, 8283-8291, http://doi.org/10.1021/acs.est.8b00890，2018.

Coble, P. G.: Marine optical biogeochemistry: The chemistry of ocean color, Chem. Rev., 107, 402-418. http://doi.org/10.1021/cr050350+, 2007.

https://doi.org/10.5194/acp-2019-1032
Preprint. Discussion started: 24 January 2020

542 Corral Arroyo, P., Bartels-Rausch, T., Alpert, P. A., Dumas, S., Perrier, S., George, C.
543 and Ammann, M.: Particle-phase photosensitized radical production and aerosol
544 aging, Environ. Sci. Technol., 52, 7680–7688,
545 https://doi.org/10.1021/acs.est.8b00329, 2018.
546 Das, T. N.: Monomer and dimer radical cations of benzene, toluene, and naphthalene,
547 J. Phys. Chem. A., 113, 6489-6493, http://doi.org/ 10.1021/jp9028408, 2009.
548 Duarte, R. M. B. O., Pio, C. A., and Duartea, A. C.: Spectroscopic study of the
549 water-soluble organic matter isolated from atmospheric aerosols collected under
550 different atmospheric conditions, Anal. Chim. Acta, 530, 7-14,
551 http://doi.org/10.1016/j.aca.2004.08.049, 2005.
552 Erickson, P. R., Moor, K. J., Werner, J. J., Latch, D. E., Arnold, W. A., and McNeill,
553 K.: Singlet Oxygen Phosphorescence as a Probe for Triplet-State Dissolved
554 Organic Matter Reactivity, Environ. Sci. Tech., 52, 9170-9178,
555 http://doi.org/10.1021/acs.est.8b02379, 2018.
556 Faust, B. C., and Allen, J. M.: Aqueous-Phase Photochemical Formation of Hydroxyl
557 Radical in Authentic Cloudwaters and Fogwaters, Environ. Sci. Tech., 27,
558 1221-1224, https://doi.org/10.1021/es00043a024, 1993.
559 Fellman, J. B., Miller, M. P., Cory, R. M., D'Amore, D. V., and White, D.:
560 Characterizing Dissolved Organic Matter Using PARAFAC Modeling of
561 Fluorescence Spectroscopy: A Comparison of Two Models, Environ. Sci. Tech.,
562 43(16), 6228-6234. https://doi.org/10.1021/es900143g, 2009.
563 Feng, Y., Ramanathan, V. and Kotamarthi, V. R.: Brown carbon: a significant
564 atmospheric absorber of solar radiation?, Atmos. Chem. Phys., 13, 8607-8612,
565 https://doi.org/10.5194/acp-13-8607-2013, 2013.
566 Gao, Y., and Zhang, Y. H.: Formation and photochemical investigation of brown
567 carbon by hydroxyacetone reactions with glycine and ammonium sulfate, RSC.
568 Adv., 8, 20719-20725, https://doi.org/10.1039/c8ra02019a, 2018.
569 Glasius, M., Ketzel, M., Wåhlin, P., Jensen, B., Mønster, J., Berkowicz, R. and
570 Palmgren, F.: Impact of wood combustion on particle levels in a residential area
571 in Denmark, Atmos. Environ., 40, 7115-7124,
572 https://doi.org/10.1016/j.atmosenv.2006.06.047, 2006.
573 Graber, E. R., and Rudich, Y.: Atmospheric HULIS: how humic-like are they? A
574 comprehensive and critical review, Atmos. Chem. Phys., 6, 980-9860,
575 https://doi.org/10.5194/acp-6-729-2006, 2005.
576 Graedel, T. E., and Weschler, C. J.: Chemistry within aqueous atmospheric aerosols
577 and raindrops, Rev. Geophys., 19, 505-539,
578 https://doi.org/10.1029/RG019i004p00505, 1981.
579 Grebel, J. E., Pignatello, J. J., and Mitch, W. A.: Sorbic acid as a quantitative probe
580 for the formation, scavenging and steady-state concentrations of the
581 triplet-excited state of organic compounds, Water Res., 45, 6535-6544.
582 https://doi.org/10.1016/j.watres.2011.09.048, 2011.
583 Helms, J. R., Stubbins, A., Ritchie, J. D., Minor, E. C., Kieber, D., and Mopper, K.:
584 Absorption spectral slopes and slope ratios as indicators of molecular weight,
585 source, and photobleaching of chromophoric dissolved organic matter, Limnol.
586 and Oceanogr., 53, 955-969, https://doi.org/10.4319/lo.2008.53.3.0955, 2008.
587 Ho, K. F., Ho, S. S. H., Lee, S. C., Cheng, Y., Chow, J. C., Watson, J. G., Louie, P. K.
588 K., and Tian, L. W.: Emissions of gas- and particle-phase polycyclic aromatic
589 hydrocarbons (PAHs) in the Shing Mun Tunnel, Hong Kong, Atmos. Environ.,
590 43, 6343-6351, https://doi.org/10.1016/j.atmosenv.2009.09.025, 2009.
591 Jacob, D. J.: Chemistry of OH in Remote Clouds and Its Role in the Production of

https://doi.org/10.5194/acp-2019-1032
Preprint. Discussion started: 24 January 2020

592 Formic Acid and Peroxymonosulfate, J. Geophys. Res., 91, 9807-9826,
593 https://doi.org/10.1029/dj091id09p09807, 1986.
594 Kaur, R., and Anastasio, C.: First Measurements of Organic Triplet Excited States in
595 Atmospheric Waters, Environ. Sci. Tech., 52, 5218-5226,
596 https://doi.org/10.1021/acs.est.7b06699, 2018.
597 Kaur, R., Labins, J. R., Helbock, S. S., Jiang, W., Bein, K. J., Zhang, Q. and
598 Anastasio, C.: Photooxidants from brown carbon and other chromophores in
599 illuminated particle extracts, Atmos. Chem. Phys., 19, 6579–6594,
600 https://doi.org/10.5194/acp-19-6579-2019, 2019.
601 Kloster, S., Mahowald, N. M., Randerson, J. T., Thornton, P. E., Hoffman, F. M.,
602 Levis, S., Lawrence, P. J., Feddema, J. J., Oleson, K. W., and Lawrence, D. M.:
603 Fire dynamics during the 20th century simulated by the Community Land Model,
604 Biogeosciences, 7, 1877-1902, https://doi.org/10.5194/bg-7-1877-2010, 2010.
605 Korak, J. A., Dotson, A. D., Summers, R. S., and Rosario-Ortiz, F. L.: Critical
606 analysis of commonly used fluorescence metrics to characterize dissolved
607 organic matter, Water Res., 49, 327-338,
608 https://doi.org/10.1016/j.watres.2013.11.025, 2014.
609 Lambe, A. T., Zhang, J. Y., Sage, A. M., and Donahue, N. M.: Controlled OH Radical
610 Production via Ozone-Alkene Reactions for Use in Aerosol Aging Studies,
611 Environ. Sci. Tech., 41, 2357-2363. https://doi.org/10.1021/es061878e, 2007.
612 Lee, S. C., Ho, K. F., Chan, L. Y., Zielinska, B., and Chow, J. C.: Polycyclic aromatic
613 hydrocarbons (PAHs) and carbonyl compounds in urban atmosphere of Hong
614 Kong, Atmos. Environ., 35, 5949-5960,
615 https://doi.org/10.1016/S1352-2310(01)00374-0, 2001.
616 Lin, P., Laskin, J., Nizkorodov, S. A., and Laskin, A.: Revealing Brown Carbon
617 Chromophores Produced in Reactions of Methylglyoxal with Ammonium
618 Sulfate, Environ. Sci. Tech., 49, 14257-14266,
619 https://doi.org/10.1021/acs.est.5b03608, 2015.
620 Lin, Y. H., Budisulistiorini, S. H., Chu, K., Siejack, R. A., Zhang, H., Riva, M.,
621 Zhang, Z. F., Gold, A., Kautzman, K. E., and Surratt, J. D.: Light-Absorbing
622 Oligomer Formation in Secondary Organic Aerosol from Reactive Uptake of
623 Isoprene Epoxydiols, Environ. Sci. Tech., 48, 12012-12021,
624 https://doi.org/10.1021/es503142b, 2014.
625 Liu, S. J., Jiang, X. T., Tsona, N. T., Lv, C., and Du, L.: Effects of NOx, SO2 and RH
626 on the SOA Formation from Cyclohexene Photooxidation, Chemosphere, 216,
627 794-804, https://doi.org/10.1016/j.chemosphere.2018.10.180, 2018.
628 Ma, C. Y., Zhuang, T., Zhang, Z. Y., Wang, J., Yang, F., Qiao, C., and Lu, M. M.:
629 Tailpipe emission characteristics of PM2.5 from selected on-road China III and
630 China IV diesel vehicles, Aerosol Science and Technology, 52, 799-808,
631 https://doi.org/10.1080/02786826.2018.1466027, 2018.
632 Ma, J. H., Del Vecchio, R., Golanoski, K. S., Boyle, E. S., and Blough, N. V.: Optical
633 Properties of Humic Substances and CDOM: Effects of Borohydride Reduction,
634 Environ. Sci. Tech., 44, 5395–5402, https://doi.org/10.1021/es100880q, 2010.
635 Manfrin, A., Nizkorodov, S. A., Malecha, K. T., Getzinger, G. J., McNeill, K. and
636 Borduas-Dedekind, N.: Reactive Oxygen Species Production from Secondary
637 Organic Aerosols: The Importance of Singlet Oxygen, Environ. Sci. Technol., 53,
638 8553–8562. https://doi.org/10.1021/acs.est.9b01609, 2019.
639 Mcdonald, J. D., Zielinska, B., Fujita, E. M., Sagebiel, J. C., Chow, J. C., and Watson,
640 J. G.: Fine particle and gaseous emission rates from residential wood combustion,
641 Environ. Sci. Tech., 34, 2080-2091, https://doi.org/10.1021/es9909632, 2000.

https://doi.org/10.5194/acp-2019-1032
Preprint. Discussion started: 24 January 2020

642 McKnight, D. M., Boyer, E. W., Westerhoff, P. K., Doran, P. T., Kulbe, T., and
643 Andersen, D. T.: Spectrofluorometric characterization of dissolved organic
644 matter for indication of precursor organic material and aromaticity, Limnol.
645 Oceanogr., 46, 38-48, https://doi.org/10.4319/lo.2001.46.1.0038, 2001.
646 McNeill, K., and Canonicab, S.: Triplet state dissolved organic matter in aquatic
647 photochemistry: Reaction mechanisms, substrate scope, and photophysical
648 properties, Environ. Sci.: Processes Impacts, 18, 1381-1399,
649 https://doi.org/10.1039/c6em00408c, 2016.
650 Moor, K. J., Schmitt, M., Erickson, P. R., and McNeill, K.: Sorbic Acid as a Triplet
651 Probe: Triplet Energy and Reactivity with Triplet-State Dissolved Organic
652 Matter via $^1O_2$ Phosphorescence, Environ. Sci. Tech., 53, 8078-8086,
653 https://doi.org/10.1021/acs.est.9b01787, 2019.
654 Munger, J. M., Jacob, D. J., Waldman, J. M., and. Hoffmann, M. R.: Fogwater
655 Chemistry in an Urban Atmosphere, J. Geophys. Res., 88, 5109-5121,
656 https://doi.org/10.1029/JC088iC09p05109, 1983.
657 Murphy, K. R., Stedmon, C. A., Waite, T. D., and Ruiz, G. M.: Distinguishing
658 between terrestrial and autochthonous organic matter sources in marine
659 environments using fluorescence spectroscopy, Marine Chem., 108, 40-58,
660 https://doi.org/10.1016/j.marchem.2007.10.003, 2008.
661 Pechony, O., and Shindell, D. T.: Driving forces of global wildfires over the past
662 millennium and the forthcoming century, Proc. Natl. Acad. Sci. USA., 107,
663 19167-19170, https://doi.org/10.1073/pnas.1003669107, 2010.
664 Peuravuori, J., and Pihlaja, K.: Molecular size distribution and spectroscopic
665 properties of aquatic humic substances, Anal. Chim. Acta, 337, 133-149,
666 https://doi.org/10.1016/S0003-2670(96)00412-6, 1997.
667 Richards-Henderson, N. K., Pham, A. T., Kirk, B. B., and Anastasio, C.: Secondary
668 Organic Aerosol from Aqueous Reactions of Green Leaf Volatiles with Organic
669 Triplet Excited States and Singlet Molecular Oxygen, Environ. Sci. Tech., 49,
670 268-276, https://doi.org/10.1021/es503656m, 2015.
671 Rogge, W. F., Hildemann, L. M., Mazurek, M. A., Cass, G. R., and Simoneit, B. R. T.:
672 Sources of Fine Organic Aerosol. 9. Pine, Oak, and Synthetic Log Combustion
673 in Residential Fireplaces, Environ. Sci. Tech., 32, 13-22,
674 https://doi.org/10.1021/es960930b, 1998.
675 Rosario-Ortiz, F. L., and Canonica, S.: Probe Compounds to Assess the
676 Photochemical Activity of Dissolved Organic Matter, Environ. Sci. Tech., 50,
677 12532-12547, https://doi.org/10.1021/acs.est.6b02776, 2016.
678 Schauer, J. J., Kleeman, M. J., Cass, G. R., and Simoneit, B. R. T.: Measurement of
679 emissions from air pollution sources. 3. C1-C29 organic compounds from
680 fireplace combustion of wood, Environ. Sci. Tech., 35, 1716-1728,
681 https://doi.org/10.1021/es001331e, 2001.
682 Schmitt, M., Moor, K. J., Erickson, P. R., and McNeill, K.: Sorbic Acid as a Triplet
683 Probe: Reactivity of Oxidizing Triplets in Dissolved Organic Matter by Direct
684 Observation of Aromatic Amine Oxidation, Environ. Sci. Tech., 53, 8087-8096,
685 https://doi.org/10.1021/acs.est.9b01789, 2019.
686 Sharpless, C. M., Macheal, A., Page, S. E., Wenk, J., Sander, M., and McNeill, k.:
687 Photooxidation-Induced Changes in Optical, Electrochemical, and
688 Photochemical Properties of Humic Substances, Environ. Sci. Tech., 48,
689 2688-2696. https://doi.org/10.1021/es403925g, 2014.
690 Shen, Z. X., Zhang, Q., Cao, J. J., Zhang, L. M., Lei, Y. L., Huang, Y., Huang, R. J.,
691 Gao, J. J., Zhao, Z. Z., Zhu, C. S., Yin, X. L., Zheng, C. L., Xu, H. M., and Liu, S.

https://doi.org/10.5194/acp-2019-1032
Preprint. Discussion started: 24 January 2020

X.: Optical properties and possible sources of brown carbon in $PM_{2.5}$ over Xi'an, China, Atmos. Environ., 150, 322-330, https://doi.org/10.1016/j.atmosenv.2016.11.024, 2017.

Smith, J. D., Sio, V., Yu, L., Zhang, Q., and Anastasio C.: Secondary Organic Aerosol Production from Aqueous Reactions of Atmospheric Phenols with an Organic Triplet Excited State, Environ. Sci. Tech., 48, 1049-1057, https://doi.org/10.1021/es4045715, 2015.

Tian, F. L., Chen, J. W., Qiao, X. L., Wang, Z., Yang, P., Wang, D. G. and Ge, L. K.: Sources and seasonal variation of atmospheric polycyclic aromatic hydrocarbons in Dalian, China: Factor analysis with non-negative constraints combined with local source fingerprints, Atmos. Environ., 43, 2747-2753, https://doi.org/10.1016/j.atmosenv.2009.02.037, 2009.

Turro, N. J., and Engel, R.: Quenching of biacetyl fluorescence and phosphorescence, J. Am. Chem. Soc., 91, 7113-7121, https://doi.org/10.1021/ja01053a073, 1969.

Wei, S. Y., Song, J. Z., Peng, P. A., and Yu, C. L.: Py-GC/MS study on the characteristics of soot and charcoal derived from biomass materials and coal, Geochimica, 46, 240-251, https://doi.org/10.3969/j.issn.0379-1726.2017.03.004, 2017.

Wenk, J., Aeschbacher, M., Sander, M., Gunten, U. V., and Canonica S.: Photosensitizing and Inhibitory Effects of Ozonated Dissolved Organic Matter on Triplet-Induced Contaminant Transformation, Environ. Sci. Tech., 49, 8541-8549, https://doi.org/10.1021/acs.est.5b02221, 2015.

Wong, J. P. S., Nenes, A. and Weber, R. J.: Changes in light absorptivity of molecular weight separated brown carbon due to photolytic aging, Environ. Sci. Technol., 51, 8414–8421, https://doi.org/10.1021/acs.est.7b01739, 2017.

Wong, J. P. S., Tsagkaraki, M., Tsiodra, I., Mihalopoulos, N., Violaki, K., Kanakidou, M., Sciare, J., Nenes, A. and Weber, R. J.: Atmospheric evolution of molecular-weight-separated brown carbon from biomass burning, Atmos. Chem. Phys., 19, 7319–7334, https://doi.org/10.5194/acp-19-7319-2019, 2019.

Wong, J. P. S., Zhou, S. M., and Abbatt, J. P. D.: Changes in Secondary Organic Aerosol Composition and Mass due to Photolysis: Relative Humidity Dependence, J. Phys. Chem., 119, 4309-4316. https://doi.org/10.1021/jp506898c, 2015.

Wu, G. M., Ram. K., Fu, P. Q., Wang, W., Zhang, Y. L., Liu, X. Y., Stone, E. A., Pradhan, B. B., Dangol, P. M., Panday, A. K., Wan, X., Bai, Z. P., Kang, S. C., Zhang, Q., G., and Cong, Z. Y.: Water-Soluble Brown Carbon in Atmospheric Aerosols from Godavari (Nepal), a Regional Representative of South Asia, Environ. Sci. Tech., 53, 3471-3479, https://doi.org/10.1021/acs.est.9b00596, 2019.

Xu, M., He, W. Q., Nie, L., Han, L. H., Pan, T., and Shi, A. J.: Atmospheric Pollutant Emission Characteristics from the Cooking Process of Traditional Beijing Roast Duck, Environ. Sci., 38, 3139-3145, https://doi.org/10.13227/j.hjkx.201701165, 2017.

Yang, B. Y., Huang, X. X., Zheng, A., Liu, B. L., and Wu, S. P.: Compositions of Organic Acids in PM_{10} Emission Sources in Xiamen Urban, Environ. Sci., 34, 8-14, 2013.

You, Y., Renbaum-Wolff, L., Carreras-Sospedra, M., Hanna, S. J., Hiranuma, N., Kamal, S., Smith, M. L.. Zhang, X. L. Weber, R. J., Shilling, J. E., Dabdub, D., Martin, S. T., and Bertram, A. K.: Images reveal that atmospheric particles can

https://doi.org/10.5194/acp-2019-1032
Preprint. Discussion started: 24 January 2020

Atmospheric Chemistry and Physics Discussions

741 undergo liquid-liquid phase separations, Proc. Natl. Acad. Sci. USA., 109,
742 13188-13191, https://doi.org/10.1073/pnas.1206414109, 2012.
743 Zepp, R. G., Schlotzhauer, P. F., and Sink, R. M: Photosensitized transformations
744 involving electronic energy transfer in natural waters: role of humic substances,
745 Environ. Sci. Tech., 19, 74-81, https://doi.org/10.1021/es00131a008, 1985.
746 Zhou, H. X., Yan, S. W., Lian, L. S., and Song. W. H.: Triplet-State Photochemistry
747 of Dissolved Organic Matter: Triplet- State Energy Distribution and Surface
748 Electric Charge Conditions, Environ. Sci. Tech., 53, 2482-2490,
749 https://doi.org/10.1021/acs.est.8b06574, 2019.